

Common surface structures of graphene and Au(111) : The effect of rotational angle on adsorption and electronic properties

Merve Yortanlı and Ersen Mete*

Department of Physics, Balıkesir University, Balıkesir 10145, Turkey

(Dated: September 10, 2019)

Graphene adsorption on Au(111) surface was explored to identify their common surface structures by means of van der Waals corrected density functional theory calculations. The alignment of graphene in the form of certain rotational angles on the gold surface has an important role on the lattice matching which causes Moiré patterns, and on the electronic properties of the resulting common cell structures. The dispersive weak interactions between carbon and gold layers lead to a downward shift of Fermi energy of the adsorption system with respect to the Dirac point of graphene showing a p -type doping character. Moreover, the shift was shown to depend on the rotational angle of graphene on Au(111).

I. INTRODUCTION

Graphene is a two dimensional material made up of carbon atoms in a hexagonal lattice arrangement. It receives a growing attention since its discovery in 2004 [1, 2], due to its unusual mechanical, thermal, electronic and optical properties (e.g. impressive mechanical strength and flexibility, high thermal conductivity, ultrahigh charge-carrier mobility, and unique optical response).[3–5]

Theoretically, graphene can be modeled as a free-standing two dimensional sheet. In this form, graphene's superior electronic conductivity is related to the conical singularities, at the corners of the hexagonal Brillouin zone, which show linear energy dispersion up to ± 1 eV from the Fermi level. These structures also known as the Dirac cones where the upper and lower conicals from the conduction and valence bands touch at the Dirac point. This gives graphene a gapless electronic structure and massless charge-carriers which lead to novel topological phenomena such as quantum spin Hall effect.[6, 7]

The growth and transfer of free-standing graphene onto metal surfaces in control-based electronic device designs brings some difficulties about scalable production, desirable quality, and practicality. Moreover, design specific functionality to graphene can be achieved either by dopants (such as boron nitride (BN) molecules, H, Al, Si, P and S atoms), or by adsorbing the graphene monolayer onto a metal surface, or even by using graphene nanostructures like nanoribbons.[8–14]

The increasing demand for functional electronic applications, such as display technologies, pushes researchers to develop substrate supported transparent conducting layers. Graphene monolayers with long-range order can be synthesized on metal surfaces via, for example, chemical vapor deposition (CVD).[15] Graphene coating on metal surfaces is an advantageous method which can be adapted to a wide range of areas such as electronics, solar

cells, optoelectronics, sensor-technology and bio-devices. [16–23]

The growth of graphene monolayers on metal foils such as Cu leads to polycrystalline films with domains depending on the crystallographic orientations. Moiré superstructures were observed on epitaxial graphene which occur due to matching of graphene lattice with that of the metal substrate depending on the periodic coincidence and the rotational angle between them.[12, 24] Wofford *et al.*[25] synthesized and observed graphene orientation in a R30 alignment on Au(111) using low-energy electron diffraction (LEED). In this study, one of the aims is to identify a number of small size common surface cell structures of graphene and gold (111) by considering possible rotational alignments. The choice of gold as the substrate has some advantages such as its low C solubility, inert surfaces to oxidation, lower vapor pressures relative to that of Cu, and re-usability.[25]

The adsorption and electronic properties of graphene/metal surface structures must be well understood for highly efficient device designs. For this reason there are many experimental studies to elaborate the mechanism of graphene adsorption on metal surfaces. [26–39] For instance, the interaction between graphene and Ti(0001), Ni, Pd and Co (111) surfaces are known to be stronger (chemisorption) relative to physisorption on Au, Ag, Pt, Al, Ru surfaces. The reasons leading to these two adsorption regimes, and their affects on the chemical and electronic properties of graphene/metal systems have been investigated by many theoretical studies.[40–57] The Dirac conical structure of graphene is less affected at the weak interfacial interaction regime. However, due to the difference in graphene and metal surface work functions, Fermi level of the total system shifts up relative to the Dirac point on Ag, Al, Cu substrates (n -type doping) or down on Au, Pt substrates (p -type doping). The upward or downward shift of Fermi level is considered to be associated with the work functions of graphene and the corresponding transition metal surface.[46, 58] In addition, the equilibrium distance between adsorbed graphene and the metal surface determines the Fermi level shift.[41] Chemisorption on

* Corresponding author : emete@balikesir.edu.tr

Ni, Pd and Co surfaces, on the other hand, is due to the strong interaction between the p_z orbitals of C atoms graphene and the d orbitals of the metal surface. In this case, the band structure of graphene changes and mixes with that of metal substrate.[40, 46]

The computational studies usually consider (2×2) supercell of graphene as the smallest common structure for graphene and metal surfaces. There is a need to determine the possible common supercell structures with different periodicities. In this study, the metal substrate has been chosen as gold. Apart from the advantageous sides of gold as a substrate for the adsorption of graphene monolayers mentioned earlier, Au(111) is a well-known surface which is encountered in many applications such as self-assembled monolayers (SAM).[59–66] In recent years, there are a few studies on the application of graphene coating on gold surface-based SAMs.[67–69] For instance, Xie *et al.* comparatively analyzed the electrochemical properties of bare gold, of gold with n-octadecyl mercaptan ($C_{18}H_{37}SH$) SAMs, and of graphene adsorbed SAM/Au system.[67] They reported that there was no electron transfer between the non-graphene/SAM structure and the ruthenium hexamine redox probe, so the material exhibited insulating behavior. However, they observed an electron transfer between the graphene coated SAM and the redox probe. In another recent study, Yan *et al.* studied the photoemission characteristics of gold surface/diamondoid SAMs covered with graphene as the stabilizer/protector layer.[69] They reported that the graphene coating prevents the desorption of diamondoid molecules from the gold surface by forming a good barrier over the diamondoid SAMs. Such applications put forward the need to determine common surface supercells of hetero-layered structures which involve Au and graphene. The combination of gold and graphene has a great potential in different types of novel designs.

We systematically investigated the matching periodicities of graphene on Au(111) to determine their several common surface cells using modern dispersion corrected DFT calculations. One of the main focuses has been given to elaboration of the adsorption geometries, interlayer binding characteristics, energy bands, and work functions of these structures. Since different common geometries are expected to show various atomic coincidences, it becomes important to explore the effect of such differences between the common periodicities on the adsorption and electronic properties of graphene on Au(111).

II. THEORETICAL METHOD

Total energy density functional theory (DFT) calculations in the framework of the projected augmented wave method (PAW) have been performed using VASP [70–73]. Single-particle orbitals were expanded in the plane wave basis up to a kinetic energy cut-off value of 400 eV. The exchange-correlation (XC) effects have been in-

cluded based on the modern and nonempirical SCAN[74] (strongly constrained and appropriately normed) semilocal meta-Generalized Gradient Approximation (meta-GGA) density functional.

To achieve more consistent results for weakly interacting layered structures, van der Waals (vdW) forces must be taken into consideration. As known from the previous studies, the interaction between Au surface and graphene layer is a weak physisorption interaction.[40, 75] Hence, we have used SCAN+rVV10 exchange-correlation functional which includes dispersive corrections through non-local correlation functional rVV10.[76] In fact, recent studies showed that the SCAN+rVV10 vdW density functional produces excellent results for interlayer binding energies of layered materials as well as the adsorption energies of graphene on transition metal surfaces.[77] In order to give a better description of the effect of the vdW-DFT approach on the computationally estimated values of the weakly interacting graphene/gold system, the results obtained by using PBE functional, which is based on the standard generalized gradient approximation (GGA), are also presented.

In addition, even though gold is a metallic system, use of different vdW functionals make a difference in the calculated lattice constant. As given in Table I, the SCAN+rVV10 functional yields the best estimation to the experimental value of 4.078 Å. [78] The in-plane lattice constant of graphene was found as 2.445 Å and 2.442 Å with PBE and SCAN+rVV10 functionals in agreement with previous studies.[46]

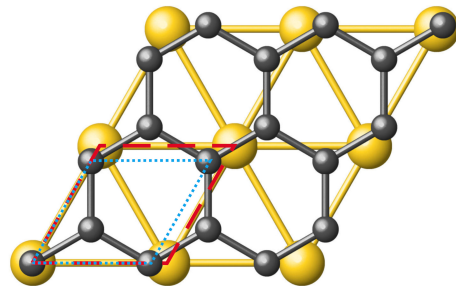


FIG. 1. Schematic representation of the graphene layer on the top layer of Au(111) surface. Dotted (blue) and dashed (red) lines indicate the unitcells of graphene and Au(111), respectively.

A four layer slab model was built to represent (111) surface of gold. Graphene is placed on gold surface such that their lattice translation vectors coincide as shown in Fig. 1. The magnitude of the in-plane translation vectors of gold and graphene were found by employing vdW corrections as 2.744 Å and 2.442 Å, respectively. Therefore, (1×1) unit cell of graphene has a 11% mismatch to that of gold. By rotating graphene monolayer on gold surface, matching supercell structures were explored. A strain of about %2 on graphene caused by adsorption on the gold surface is imposed as a criteria to identify common supercells. The strain percentage on graphene is calculated

TABLE I. Comparison of the bulk Au lattice constant between experimental and various XC functionals values.

Method	Au lattice constant (Å)
Exp.[78]	4.078
LDA	4.052
PBE	4.156
PBE-DF2	4.330
PBE+dDsC	4.110
SCAN	4.095
SCAN+rVV10	4.073

using,

$$\frac{d_{C-C}^{\text{free}} - d_{C-C}^{\text{adsorbed}}}{d_{C-C}^{\text{free}}} \times 100$$

where d_{C-C}^{free} and $d_{C-C}^{\text{adsorbed}}$ are the C-C bond lengths in free-standing and adsorbed graphene monolayers.

Each of the computational cells consists of a four layer gold slab with a graphene adsorption monolayer obeying the same periodicity, and a 12Å thick vacuum region to prevent any unphysical interaction between the periodic images of the slabs. Methfessel-Paxton smearing with $\sigma = 0.05$ was used in the calculations. Atomic coordinates were optimized self-consistently until Hellman-Feynmann forces acting on each atom at each of the three cartesian directions became less than 10^{-2} eV/Å. No atom was frozen to its bulk position. In the geometry optimizations, surface Brillouin zone (BZ) integrals were carried out by k -point samplings which were chosen properly to be dense enough for a metallic system and to be compatible with the translational symmetry of the corresponding reciprocal cell. In the structure optimizations we switched off the symmetry operations which reduces the number of k -points in the irreducible BZ. For example, Γ -centered $6 \times 6 \times 1$ k -point grid was used for the (4×4) computational cell which has a hexagonal symmetry. The naming of the common supercell structures is hereinafter adapted with respect to the (111) surface of gold. Similarly, an $8 \times 8 \times 1$ k -point mesh was chosen for (3×3) and $(\sqrt{7} \times \sqrt{7})R19.12^\circ$ supercells. For the $(\sqrt{3} \times \sqrt{3})R30^\circ$ structure $10 \times 10 \times 1$ k -point sampling was enough to get energy values converged to a few meVs. In the relaxation of the (7×7) superstructure, the BZ integrations were performed over a $4 \times 4 \times 1$ k -point grid.

In order to describe the physisorption of a graphene monolayer on Au(111) with different possible common periodicities, the average adsorption energy E_{ads} per carbon can be obtained using the following formula,

$$E_{\text{ads}} = (E_{G/Au(111)} - E_{Au(111)} - E_G)/n$$

where $E_{G/Au(111)}$ is the total cell energy of graphene physisorbed Au(111) slab. $E_{Au(111)}$ and E_G are the energies of clean gold surface model and the graphene monolayer,

respectively. In addition n in the denominator is the number of carbon atoms contained in the computational cell.

III. RESULTS AND DISCUSSION

A. Geometry and Adsorption

Common periodic structures of graphene/Au(111) were modeled by overlapping the lattice vectors of gold and graphene unit cells, and then rotating the graphene monolayer on the Au(111) surface. The in-plane lattice vectors and initial configuration of both structures are shown in Fig. 1. In this position, a common superstructure can be obtained which corresponds to graphene/Au(111)- $(9 \times 9)/(8 \times 8)$ supercell. Due to its large size we did not include this geometry in this study. When the graphene monolayer is rotated 30° clockwise (or even counterclockwise) with respect to the in-plane lattice vectors of gold, it becomes commensurate with the (3×3) gold surface supercell (in Fig. 2c). We refer this geometry as (3×3) -GR 30° indicating that graphene has a rotational angle of 30° on Au(111) with a common periodicity of (3×3) cell with respect to the gold surface. LEED experiments confirmed the existence of this R30 alignment structure.[25] At this rotational angle, other common superstructures of $(3 \times \sqrt{3})$ -GR 30° and $(\sqrt{3} \times \sqrt{3})R30^\circ$ -GR 30° can be identified as given in Fig. 2a and Fig. 2b with slightly different mismatch values. In particular, $(\sqrt{3} \times \sqrt{3})R30^\circ$ -GR 30° gold surface cell (Fig. 2a) matches with (2×2) supercell of graphene. The strain ratios for these three geometries are all about -0.4% with the PBE and -2% with the SCAN+rVV10 functionals as shown in Table II where negative strain refers to shrinking.

Since the angle between the in-plane lattice vectors (or rows of gold atoms) of gold is 60° giving a hexagonal arrangement, rotation of graphene monolayer by an angle of 10° or 50° results in the same geometry. Therefore, graphene/Au(111) (4×4) superstructure shown in Fig 2d can either be called as (4×4) -GR 10° or equivalently as (4×4) -GR 50°

A larger, common geometry was identified at a rotational angle of 19.12° with a periodicity of (7×7) on the gold surface as depicted in Fig. 2f. At this rotational angle, another graphene/Au(111) superstructure can be identified with a slightly different mismatch value as $(\sqrt{7} \times \sqrt{7})R19.12^\circ$ -GR 19.12° (in Fig. 2e). Consequently, a total of six different common supercells were determined with low mismatch allowing probable Moiré patterns.

Equilibrium distances and strain ratios of graphene monolayer on Au(111) surface were calculated using the PBE and the SCAN+rVV10 functionals, and presented in Table II. The height of graphene monolayer from the topmost gold plane represents an average value over the separation distances of carbon atoms from the

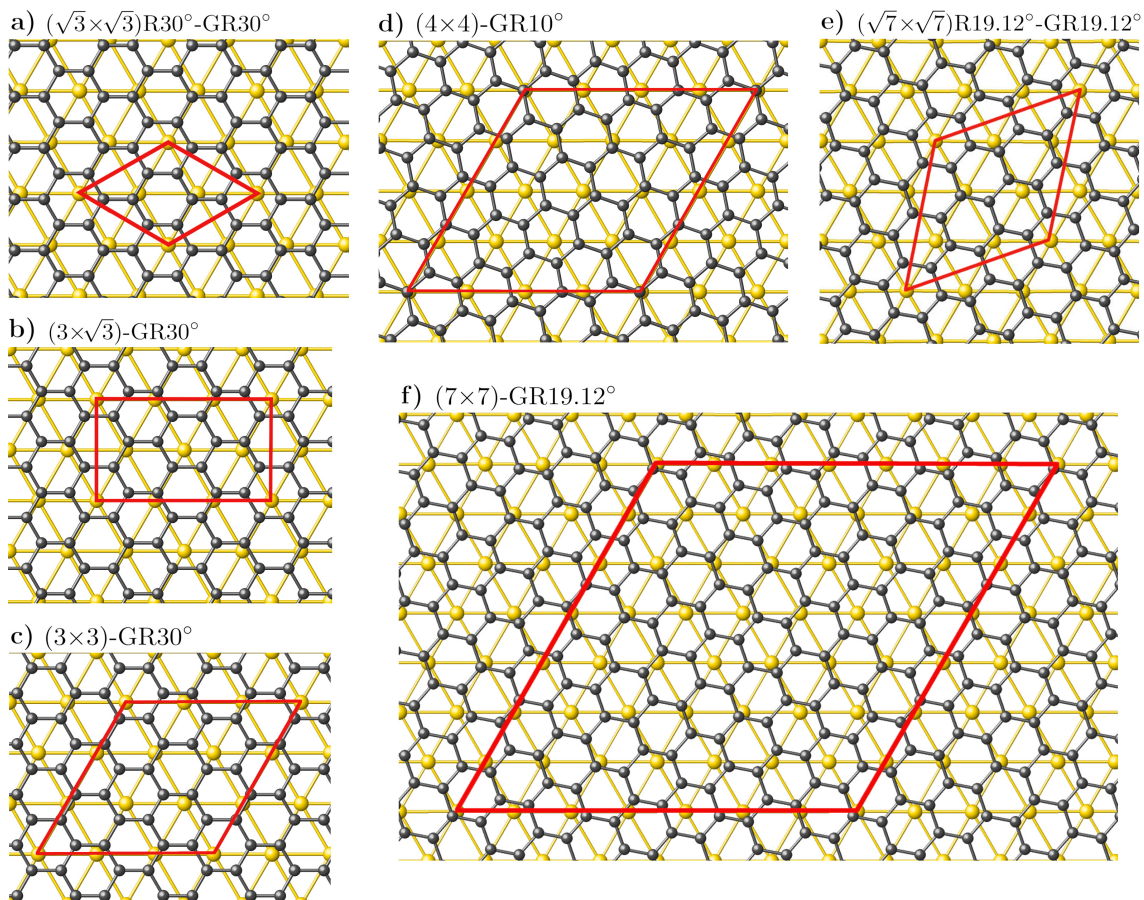


FIG. 2. (a) DFT-optimized common surface structures of graphene on gold (111) using the SCAN+rVV10 XC functional. The periodic supercell geometries were indicated by red (solid) lines. The labeling of common superstructures follows that of Au(111) on the left, a dash in the middle, and the rotational angle of graphene on the right.

TABLE II. Minimum energy heights of graphene on Au(111) surface and the ratios of strain due to mismatch of graphene monolayer with Au(111) surface cell. Negative strain rates represent shrinking.

Structure	PBE		SCAN+rVV10	
	h (Å)	strain (%)	h (Å)	strain (%)
$(\sqrt{3} \times \sqrt{3})R30^\circ-GR30^\circ$	4.260	-0.411	3.476	-2.019
$(3 \times \sqrt{3})-GR30^\circ$	4.266	-0.472	3.480	-2.024
$(3 \times 3)-GR30^\circ$	4.258	-0.404	3.480	-1.989
$(4 \times 4)-GR10^\circ$	4.238	0.377	3.459	-1.244
$(\sqrt{7} \times \sqrt{7})R19.12^\circ-GR19.12^\circ$	4.223	1.409	3.448	-0.228
$(7 \times 7)-GR19.12^\circ$	4.218	1.116	3.443	-0.190

gold surface layer. It is ranging between 4.266 Å and 4.218 Å when calculated using the standard GGA XC functional. The SCAN+rVV10 functional not only includes vdW corrections but also improves the description of many-body exchange-correlation effects. Therefore, the height values become significantly smaller relative to those predicted by DFT-PBE calculations, ranging between 3.480 Å and 3.443 Å. Previous vdW-DFT

studies reported closely similar values using different vdW functionals.[44, 46, 58, 79, 80] We also note that some theoretical studies labeled the physisorption geometries with respect to graphene unit cell. For instance, Hamada *et al.*[44], and Khomyakov *et al.*[46] labeled graphene/Au(111) adsorption geometries using (1×1) and (2×2) graphene supercells.

Graphene is known to exhibit physisorption on the

TABLE III. Average adsorption energy per C atom (E_{ads}), the work function of graphene, Au(111) and graphene coated gold surface (Φ), the shift of the Dirac point of graphene with respect to the Fermi energy of the Au(111)/G system (ΔE_F), the amount of charge (per C atom) displaced from graphene to gold (ΔQ), calculated using the PBE and SCAN+rVV10 DFT functionals. Labeling of common structures of graphene and gold was made with respect to the surface unit cell of Au(111).

Structure	PBE		SCAN+rVV10			
	E_{ads} (meV)	Φ (eV)	E_{ads} (meV)	ΔE_F (eV)	Φ (eV)	ΔQ
$(\sqrt{3}\times\sqrt{3})\text{R}30^\circ\text{-GR}30^\circ$	-1.64	4.85	-62.66	+0.18	5.17	0.00604e
$(3\times\sqrt{3})\text{-GR}30^\circ$	-2.51	4.84	-64.74	+0.17	5.16	0.00660e
$(3\times 3)\text{-GR}30^\circ$	-2.47	4.86	-64.63	+0.16	5.15	0.00623e
$(4\times 4)\text{-GR}10^\circ$	-2.54	4.85	-65.00	+0.26	5.16	0.00522e
$(\sqrt{7}\times\sqrt{7})\text{R}19.12^\circ\text{-GR}19.12^\circ$	-6.02	4.86	-70.13	+0.34	5.12	0.00710e
$(7\times 7)\text{-GR}19.12^\circ$	-6.08	4.86	-72.18	+0.38	5.12	0.00759e
Graphene	-	4.48	-	-	4.58	-
Au(111)	-	5.12	-	-	5.45	-

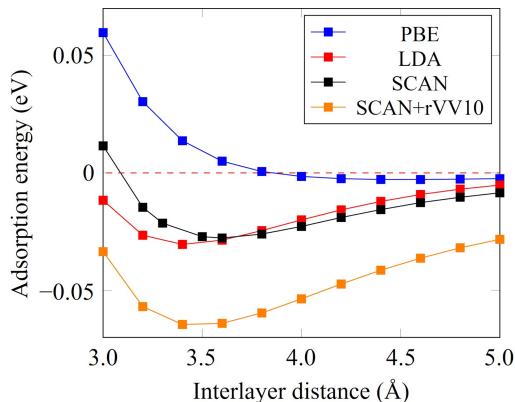


FIG. 3. Comparison of the adsorption energy (per C atom) profiles, calculated with different XC functionals, as a function of the interlayer distance between the graphene layer and the gold (111)-(4×4) surface.

gold surface. [12, 79] In order to show the role of the vdW effects on the estimated values, we obtained the adsorption energy (per C atom) profiles as a function of the graphene/Au(111) interlayer distance using different XC functionals as shown in Fig. 3. In these calculations, the distance of graphene monolayer from the gold surface was changed stepwise and no relaxation was performed. The PBE functional severely underestimates the adsorption energy. The standard GGA functionals are not suitable for chemisorption on metal systems either. For instance, even though the interaction between graphene and Ni(111) show a chemisorption behavior, PBE results suggest physisorption.[52] The SCAN and LDA functionals give a relatively better but not sufficiently strong interaction between graphene and gold substrate. When the SCAN functional is supplemented with the rVV10 vdW corrections, a significant improvement can be obtained on both the adsorption energy and the equilibrium distance.

In addition, the adsorption energy profile for the PBE functional gets almost insensitive to interlayer distance after ~ 4.2 Å. Therefore, the PBE-predicted heights do not show a correlation with the strain ratios of graphene on gold. On the other hand, vdW-DFT results indicate a strong correlation between the height and the strain ratios as seen in Table. II. The factors mentioned above necessitates the inclusion of dispersive forces in the theoretical calculations involving weakly interacting layered materials like graphene/Au(111).

Calculated adsorption energies per carbon atom are given in Table III. The PBE functional tends to underestimate the binding to a few meVs due to lack of long-range dispersive interactions as expected. The adsorption energies of a single layer graphene on the gold surface given by Zheng *et al.*[58] for the PBE functional are in excellent agreement with our results in Table III. On the other hand, vdW corrections bring a significant improvement over the energy related estimations. The interaction of graphene on the metal is relatively weak with $E_{\text{ads}}=-62.66$ meV at the $(\sqrt{3}\times\sqrt{3})\text{R}30^\circ\text{-GR}30^\circ$ superstructure and gets stronger with the increasing supercell size up to $E_{\text{ads}}=-72.18$ meV at the $(7\times 7)\text{-GR}19.12^\circ$ superstructure. The latter adsorption energy is in good agreement with a previous result obtained using DFT-D3 method.[79] Depending on the choice of the vdW functional scheme, the corresponding estimations may slightly vary. Our adsorption energy values calculated using the SCAN+rVV10 functional gives a reasonable agreement with previous theoretical estimations.[57, 58] The differences in the calculated adsorption energies between computational studies regarding the graphene/Au(111) system can be attributed to the use of different supercell structures and the vdW method. Another important factor appears to be the lack of rotational angular orientation of graphene on the gold surface in the previous studies. For instance, Tesch *et al.* considered the same alignment of graphene on both (2×2) and (7×7) graphene supercells which

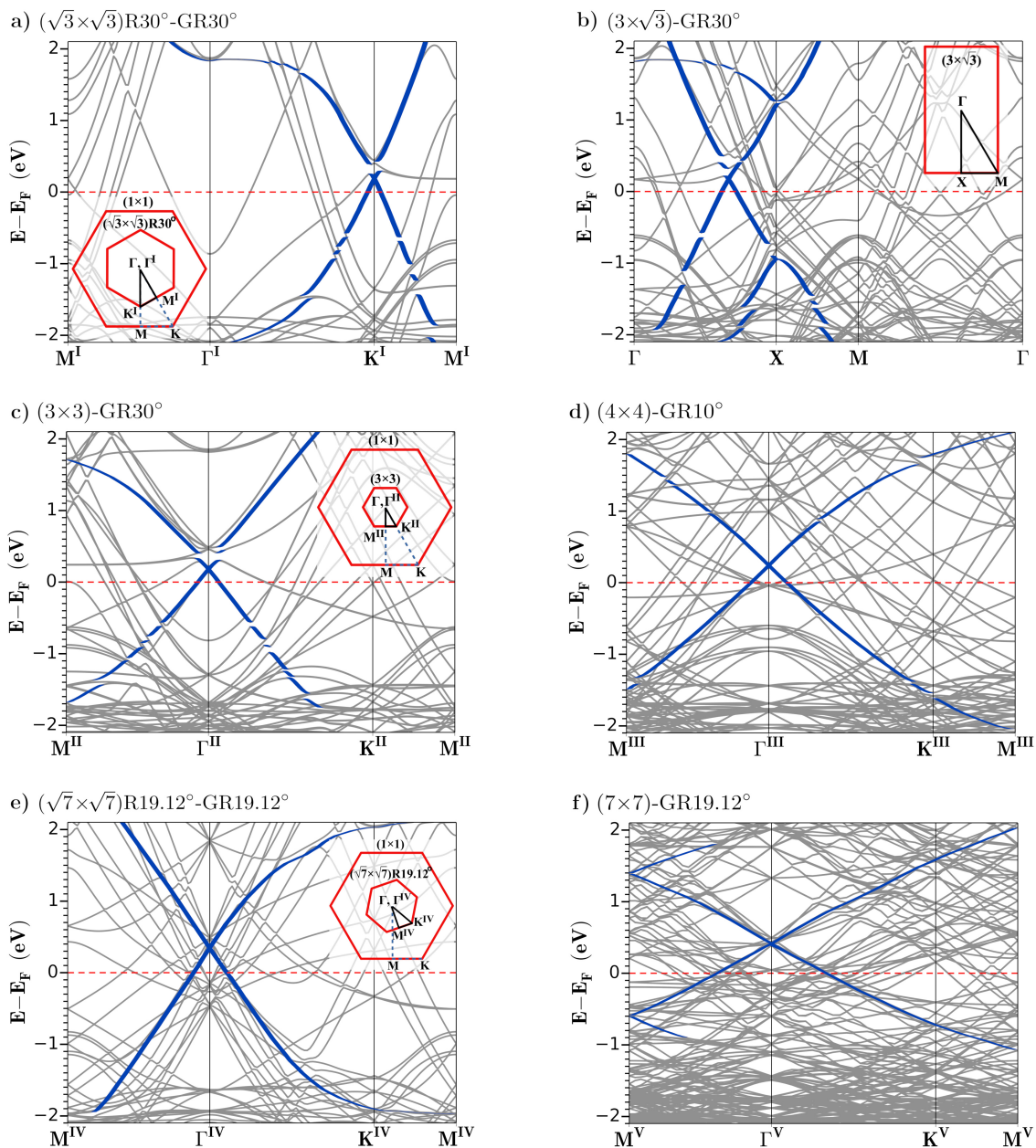


FIG. 4. Electronic band structures of graphene monolayer on Au(111) with identified common superstructures. The corresponding two-dimensional BZ and high-symmetry points are depicted in the insets. The contributions from graphene p_z orbitals are highlighted with blue color (thick dark bands). The energy values are given relative to the Fermi level (dashed lines) of each adsorption system.

correspond to $(\sqrt{3} \times \sqrt{3})R30^\circ$ and (6×6) gold surface supercells, respectively. In our optimization calculations graphene gets bulged on (6×6) gold surface therefore we did not include this case.

As a result, the graphene/metal interlayer distance is sensitive to the rotational angle/alignment of graphene monolayer on the metal surface. Moreover, adsorption energies also show an almost linear correlation with the interlayer distances computed with the SCAN-rVV10 functional.

B. Electronic Structures

The electronic band structures of corresponding common graphene/Au(111) systems were obtained using the SCAN+rVV10 functional as shown in Fig. 4. The Brillouin zone shapes, high symmetry points and the k -paths are shown in the insets. The size and the rotational alignment of the corresponding BZ are also depicted relative to the hexagonal BZ of the (1×1) surface unit cell of gold.

It must be noted that the k -points (Γ , K, M, and X) are given with respect to the BZ of gold supercell. There is also inward folding of the BZ when the real space periodicity increases. Therefore, the conicals not always appear at the K point of graphene unitcell. In addition, the BZ shapes of hexagonal (3×3), (4×4), and (7×7) supercells are similar. They only get smaller in size with increasing supercell size in the real space.

The weak interfacial interactions represented by vdW corrections showed that the Dirac conicals are preserved. The linear dispersion of graphene bands within ± 1 eV vicinity of the Dirac points of conicals can still be seen in all of the graphene adsorption orientations considered in this work. Moreover, graphene-metal interaction is weak such that it does not cause a band gap opening for the graphene monolayer. Then, the Dirac conicals differ in the position of the Fermi-level relative to the Dirac points. For a free-standing graphene, the Fermi-energy must be at the Dirac point. When graphene gets closer to the Au(111) surface a Fermi-level shift is observed. The downward shift of Fermi energy with respect to the Dirac point corresponds to a p -type doping of graphene monolayer.

The Fermi energy shift (with respect to the Dirac point) was found as +0.18 eV for $\sqrt{3} \times \sqrt{3}$ -R30°-GR30° using the SCAN+rVV10 functional. This result is in good agreement with a previous value of +0.19 eV for the same structure.[46] Vanin *et al.* estimated a shift of +0.21 eV by using the vdW-DF method. Tesch *et al.*[79] synthesized graphene nanoflakes on Au(111) and reported a p -type doping with a Fermi energy shift of 0.24 ± 0.07 eV.[79] Similarly, Zheng *et al.* reported a Fermi-level shift of 0.230 eV for the bilayer graphene which is also reasonably close to the calculated values presented in this work. Our results for the R30° alignment structures, (3×3)-GR30° and ($3 \times \sqrt{3}$)-GR30°, the shift values are similar because they all reflect essentially the same surface characteristics.

Ślawińska *et al.*[42] used scanning tunneling spectroscopy (STS) to show that Fermi-level shift ranges between 0.25 and 0.55 eV on different p -type doping domains of graphene on the (111) surface of gold. Our results for the graphene/Au(111) physisorption systems, indicate that the shift changes with the rotational alignment of graphene on the metal surface. The largest shift is calculated for the R19.12° alignment. The equilibrium distances of the graphene/Au(111) structures are still large for a charge transfer from graphene to gold surface. Then, we calculated Bader charges on graphene and on metal slab before and after adsorption for each of the structures considered in this work. Calculated charge transfer values from the graphene monolayer to the gold substrate are very small and only slightly larger in the case of R19.12° structures. Hence, a charge transfer model may not fully explain the Fermi-level shift mechanism. Our results rather suggest a charge redistribution induced by graphene-metal interlayer interactions.

The change in the Fermi-level shift between different

common graphene/Au(111) geometries can be attributed to the rotational angle. Because, different angles cause different atomic coincidences of C atoms with the surface gold atoms. This also leads to a change in the ratio of the number of C atoms to the number of surface Au atoms ($n_{C/Au}$) contained in the supercell. This ratio is $n_{C/Au}=2.67$, 2.63, and 2.57 at the rotational angles of 30°, 10°, and 19.12°, respectively.

Another factor affecting the Fermi-level shift can be the work function of graphene/Au(111). Theoretical studies usually explain the shift as the difference between the work functions of metal surface and graphene monolayer. Therefore, we calculated the work functions of common superstructures. The real space potential energy profiles of the common hetero-layered structures were obtained along the [111] direction. Then the work function is the difference between the Fermi energy of the combined system and the vacuum level. Experimental work function of graphene and the gold surface is ~ 4.62 eV.[81, 82] and 5.31 eV, respectively. Our SCAN+rVV10 functional estimation of 5.45 eV for the clean gold surface is in good agreement with recent theoretical values.[83] The PBE functional, on the other hand, gives a value of 5.12 eV for Au(111). Graphene monolayer is estimated to have a work function of 4.58 eV and 4.48 eV with and without the vdW-corrections, respectively. Calculated work function values of graphene coated gold surface show a significant reduction relative to the that of the clean gold surface. Furthermore, our results does not show a meaningful trend to relate with the Fermi-energy shifts. On the other hand, the Φ values for different structures all exhibit similar characteristics. Therefore, the work functions of graphene/Au(111) systems appear to be independent of graphene monolayer orientation on the gold surface. Interestingly, Song *et al.* recently reported that graphene in contact with Au gets an intermediate work function value and still dominantly show features of graphene.[81] The theoretically estimated work function values of the graphene/Au(111) superstructures assume an intermediate value and not pinned to the work function of the metal.

IV. CONCLUSIONS

We have identified a number of small-sized common graphene/Au(111) superstructures by matching their corresponding supercells. Structural optimizations and electronic properties were obtained by performing DFT calculations. The weak interaction at graphene-gold interfaces necessitates the inclusion of vdW corrections. The standard GGA functionals tend to severely underestimate adsorption energies. The common geometries show different equilibrium distances between the graphene monolayer and the gold surface depending on the rotational orientation between them.

Graphene adsorption on gold does not destroy the Dirac conicals which still show linear dispersion within

± 1 eV vicinity of the Dirac points. A change in the Fermi energy indicate p -type doping of graphene when adsorbed on the metal. Most importantly, we showed that the Fermi-level shifts depend on the rotational alignment of the graphene on the gold surface.

Consequently, the results showed that the adsorption and electronic properties of graphene/Au(111) system are sensitive to the matching of graphene monolayer to the geometry of the gold surface at different rotational angles. This would allow a tunability of characteristics of potential applications based on graphene/metal layered materials. The common superstructures identified in this study are useful and serve as building blocks to

construct and design novel hetero-layered materials involving graphene and Au(111).

ACKNOWLEDGEMENTS

This study was supported by Tubitak, The Scientific and Technological Research Council of Turkey, under Grant No. 116F174. The calculations were performed on the High Performance and Grid Computing Center (TRUBA). The authors also acknowledge financial support from Balıkesir University under Grant No. BAP 2018/039.

-
- [1] K. S. Novoselov, A. K. Geim, S. V. Morozov, D. Jiang, Y. Zhang, S. V. Dubonos, I. V. Grigorieva, and A. A. Firsov, *Science* **306**, 666 (2004).
- [2] K. S. Novoselov, A. K. Geim, S. V. Morozov, D. Jiang, M. I. Katsnelson, I. V. Grigorieva, S. V. Dubonos, and A. A. Firsov, *Nature* **438**, 197 (2005).
- [3] R. R. Nair, P. Blake, A. N. Grigorenko, K. S. Novoselov, T. J. Booth, T. Stauber, N. M. R. Peres, and A. K. Geim, *Science* **320**, 13081308 (2008).
- [4] K. V. Sreekanth, S. Zeng, J. Shang, K.-T. Yong, and T. Yu, *Scientific Reports* **2**, 737 (2012).
- [5] K. Bolotin, K. Sikes, Z. Jiang, M. Klima, G. Fudenberg, J. Hone, P. Kim, and H. Stormer, *Solid State Communications* **146**, 351355 (2008).
- [6] C. L. Kane and E. J. Mele, *Phys. Rev. Lett.* **95**, 226801 (2005).
- [7] A. H. Castro Neto, F. Guinea, N. M. R. Peres, K. S. Novoselov, and A. K. Geim, *Rev. Mod. Phys.* **81**, 109 (2009).
- [8] S. Y. Zhou, G.-H. Gweon, A. V. Fedorov, P. N. First, W. A. de Heer, D.-H. Lee, F. Guinea, A. H. Castro Neto, and A. Lanzara, *Nature Materials* **6**, 770 (2007).
- [9] L. Ci, L. Song, C. Jin, D. Jariwala, D. Wu, Y. Li, A. Srivastava, Z. F. Wang, K. Storr, L. Balicas, and et al., *Nature Materials* **9**, 430 (2010).
- [10] P. A. Denis, *Chemical Physics Letters* **492**, 251 (2010).
- [11] R. Balog, B. Jørgensen, L. Nilsson, M. Andersen, E. Rienks, M. Bianchi, M. Fanetti, E. Lægsgaard, A. Baraldi, S. Lizzit, and et al., *Nature Materials* **9**, 315319 (2010).
- [12] J. Wintterlin and M.-L. Bocquet, *Surface Science* **603**, 1841 (2009).
- [13] M. Y. Han, B. Özyilmaz, Y. Zhang, and P. Kim, *Phys. Rev. Lett.* **98**, 206805 (2007).
- [14] Y.-C. Chen, D. G. de Oteyza, Z. Pedramrazi, C. Chen, F. R. Fischer, and M. F. Crommie, *ACS Nano* **7**, 6123 (2013).
- [15] M. H. Kang, L. O. Prieto Lopez, B. Chen, K. Teo, J. A. Williams, W. I. Milne, and M. T. Cole, *ACS Applied Materials & Interfaces* **8**, 22506 (2016).
- [16] T.-H. Han, Y. Lee, M.-R. Choi, S.-H. Woo, S.-H. Bae, B. H. Hong, J.-H. Ahn, and T.-W. Lee, *Nature Photonics* **6**, 105 (2012).
- [17] J. B. Oostinga, H. B. Heersche, X. Liu, A. F. Morpurgo, and L. M. K. Vandersypen, *Nature Materials* **7**, 151 (2007).
- [18] X. Li, W. Cai, J. An, S. Kim, J. Nah, D. Yang, R. Piner, A. Velamakanni, I. Jung, E. Tutuc, S. K. Banerjee, L. Colombo, and R. S. Ruoff, *Science* **324**, 1312 (2009).
- [19] A. Reina, X. Jia, J. Ho, D. Nezich, H. Son, V. Bulovic, M. S. Dresselhaus, and J. Kong, *Nano Letters* **9**, 30 (2009).
- [20] R. Nouchi, M. Shiraishi, and Y. Suzuki, *Applied Physics Letters* **93**, 152104 (2008).
- [21] O. Salihoglu, S. Balci, and C. Kocabas, *Applied Physics Letters* **100**, 213110 (2012).
- [22] K. Kim, J.-Y. Choi, T. Kim, S.-H. Cho, and H.-J. Chung, *Nature* **479**, 338 (2011).
- [23] S. Lin, Y. Lu, J. Xu, S. Feng, and J. Li, *Nano Energy* **40**, 122 (2017).
- [24] P. Merino, M. vec, A. L. Pinardi, G. Otero, and J. A. Martn-Gago, *ACS Nano* **5**, 5627 (2011).
- [25] J. M. Wofford, E. Starodub, A. L. Walter, S. Nie, A. Bostwick, N. C. Bartelt, K. Thirmer, E. Rotenberg, K. F. McCarty, and O. D. Dubon, *New Journal of Physics* **14**, 053008 (2012).
- [26] I. Pletikosić, M. Kralj, P. Pervan, R. Brako, J. Coraux, A. T. N'Diaye, C. Busse, and T. Michely, *Phys. Rev. Lett.* **102**, 056808 (2009).
- [27] S.-Y. Kwon, C. V. Ciobanu, V. Petrova, V. B. Shenoy, J. Bareo, V. Gambin, I. Petrov, and S. Kodambaka, *Nano Letters* **9**, 3985 (2009).
- [28] H. Vita, S. Bttcher, K. Horn, E. N. Voloshina, R. E. Ovcharenko, T. Kampen, A. Thissen, and Y. S. Dedkov, *Scientific Reports* **4** (2014).
- [29] Y. S. Dedkov, A. M. Shikin, V. K. Adamchuk, S. L. Molodtsov, C. Laubschat, A. Bauer, and G. Kaindl, *Phys. Rev. B* **64**, 035405 (2001).
- [30] S. Marchini, S. Günther, and J. Wintterlin, *Phys. Rev. B* **76**, 075429 (2007).
- [31] V. M. Karpan, G. Giovannetti, P. A. Khomyakov, M. Talanana, A. A. Starikov, M. Zwierzycki, J. van den Brink, G. Brocks, and P. J. Kelly, *Phys. Rev. Lett.* **99**, 176602 (2007).
- [32] M. Gao, Y. Pan, C. Zhang, H. Hu, R. Yang, H. Lu, J. Cai, S. Du, F. Liu, and H.-J. Gao, *Applied Physics Letters* **96**, 053109 (2010).
- [33] C. Enderlein, Y. S. Kim, A. Bostwick, E. Rotenberg, and K. Horn, *New Journal of Physics* **12**, 033014 (2010).

- [34] W. Moritz, B. Wang, M.-L. Bocquet, T. Brugger, T. Greber, J. Wintterlin, and S. Günther, *Phys. Rev. Lett.* **104**, 136102 (2010).
- [35] A. Varykhalov, J. Sánchez-Barriga, A. M. Shikin, C. Biswas, E. Vescovo, A. Rybkin, D. Marchenko, and O. Rader, *Phys. Rev. Lett.* **101**, 157601 (2008).
- [36] P. W. Sutter, J.-I. Flege, and E. A. Sutter, *Nature Materials* **7**, 406 (2008).
- [37] P. Sutter, J. T. Sadowski, and E. Sutter, *Phys. Rev. B* **80**, 245411 (2009).
- [38] Z. Klusek, P. Dabrowski, P. Kowalczyk, W. Kozlowski, W. Olejniczak, P. Blake, M. Szybowicz, and T. Runka, *Applied Physics Letters* **95**, 113114 (2009).
- [39] D. Eom, D. Prezzi, K. T. Rim, H. Zhou, M. Lefenfeld, S. Xiao, C. Nuckolls, M. S. Hybertsen, T. F. Heinz, and G. W. Flynn, *Nano Letters* **9**, 2844 (2009).
- [40] G. Giovannetti, P. A. Khomyakov, G. Brocks, V. M. Karpan, J. van den Brink, and P. J. Kelly, *Phys. Rev. Lett.* **101**, 026803 (2008).
- [41] J. Sławińska, P. Dabrowski, and I. Zasada, *Phys. Rev. B* **83**, 245429 (2011).
- [42] J. Sławińska, I. Wlasny, P. Dabrowski, Z. Klusek, and I. Zasada, *Phys. Rev. B* **85**, 235430 (2012).
- [43] G. Bertoni, L. Calmels, A. Altibelli, and V. Serin, *Phys. Rev. B* **71**, 075402 (2005).
- [44] I. Hamada and M. Otani, *Phys. Rev. B* **82**, 153412 (2010).
- [45] C. Gong, G. Lee, B. Shan, E. M. Vogel, R. M. Wallace, and K. Cho, *Journal of Applied Physics* **108**, 123711 (2010).
- [46] P. A. Khomyakov, G. Giovannetti, P. C. Rusu, G. Brocks, J. van den Brink, and P. J. Kelly, *Phys. Rev. B* **79**, 195425 (2009).
- [47] M. H. Kang, S. C. Jung, and J. W. Park, *Phys. Rev. B* **82**, 085409 (2010).
- [48] R. Brako, D. okevi, P. Lazi, and N. Atodiresei, *New Journal of Physics* **12**, 113016 (2010).
- [49] S. M. Kozlov, F. Viñes, and A. Görling, *The Journal of Physical Chemistry C* **116**, 7360 (2012).
- [50] J. C. W. Swart, E. van Steen, I. M. Ciobc, and R. A. van Santen, *Phys. Chem. Chem. Phys.* **11**, 803 (2009).
- [51] B. Uchoa, C.-Y. Lin, and A. H. Castro Neto, *Phys. Rev. B* **77**, 035420 (2008).
- [52] M. Fuentes-Cabrera, M. I. Baskes, A. V. Melechko, and M. L. Simpson, *Physical Review B* **77**, 035405 (2008).
- [53] M. M. Ugeda, D. Fernández-Torre, I. Brihuega, P. Pou, A. J. Martínez-Galera, R. Pérez, and J. M. Gómez-Rodríguez, *Phys. Rev. Lett.* **107**, 116803 (2011).
- [54] Z. Xu and M. J. Buehler, *Journal of Physics: Condensed Matter* **22**, 485301 (2010).
- [55] M. Vanin, J. J. Mortensen, A. K. Kelkkanen, J. M. Garcia-Lastra, K. S. Thygesen, and K. W. Jacobsen, *Phys. Rev. B* **81**, 081408(R) (2010).
- [56] W. Zhao, S. M. Kozlov, O. Hfert, K. Gotterbarm, M. P. A. Lorenz, F. Vies, C. Papp, A. Grling, and H.-P. Steinrck, *The Journal of Physical Chemistry Letters* **2**, 759 (2011).
- [57] M. Andersen, L. Hornekær, and B. Hammer, *Phys. Rev. B* **86**, 085405 (2012).
- [58] J. Zheng, Y. Wang, L. Wang, R. Quhe, Z. Ni, W.-N. Mei, Z. Gao, D. Yu, J. Shi, and J. Lu, *Scientific Reports* **3**, 2081 (2013).
- [59] P. A. DiMilla, J. P. Folkers, H. A. Biebuyck, R. Haerter, G. P. Lopez, and G. M. Whitesides, *Journal of the American Chemical Society* **116**, 2225 (1994).
- [60] A. Kumar, H. A. Biebuyck, and G. M. Whitesides, *Langmuir* **10**, 1498 (1994).
- [61] C. B. Gorman, H. A. Biebuyck, and G. M. Whitesides, *Langmuir* **11**, 2242 (1995).
- [62] M. Mrksich, L. E. Dike, J. Tien, D. E. Ingber, and G. M. Whitesides, *Experimental cell research* **235**, 305 (1997).
- [63] H. Yamada, H. Imahori, Y. Nishimura, I. Yamazaki, T. K. Ahn, S. K. Kim, D. Kim, and S. Fukuzumi, *Journal of the American Chemical Society* **125**, 9129 (2003).
- [64] J. H. Schön, H. Meng, and Z. Bao, *Nature* **413**, 713 (2001).
- [65] N. K. Chaki and K. Vijayamohanan, *Biosensors and Bioelectronics* **17**, 1 (2002).
- [66] R. Lao, S. Song, H. Wu, L. Wang, Z. Zhang, L. He, and C. Fan, *Analytical chemistry* **77**, 6475 (2005).
- [67] X. Xie, K. Zhao, X. Xu, W. Zhao, S. Liu, Z. Zhu, M. Li, Z. Shi, and Y. Shao, *The Journal of Physical Chemistry C* **114**, 14243 (2010).
- [68] B. Li, M. Famili, E. Pensa, I. Grace, N. J. Long, C. Lambert, T. Albrecht, and L. F. Cohen, *Nanoscale* **10**, 19791 (2018).
- [69] H. Yan, K. T. Narasimha, J. Denlinger, F. H. Li, S.-K. Mo, J. N. Hohman, J. E. Dahl, R. M. Carlson, B. A. Tkachenko, A. A. Fokin, *et al.*, *Nano letters* **18**, 1099 (2018).
- [70] G. Kresse and J. Hafner, *Phys. Rev. B* **47**, 558 (1993).
- [71] G. Kresse and J. Furthmüller, *Phys. Rev. B* **54**, 11169 (1996).
- [72] G. Kresse and D. Joubert, *Phys. Rev. B* **59**, 1758 (1999).
- [73] P. E. Blöchl, *Phys. Rev. B* **50**, 17953 (1994).
- [74] J. Sun, A. Ruzsinszky, and J. P. Perdew, *Phys. Rev. Lett.* **115**, 036402 (2015).
- [75] S. Nie, N. C. Bartelt, J. M. Wofford, O. D. Dubon, K. F. McCarty, and K. Thürmer, *Phys. Rev. B* **85**, 205406 (2012).
- [76] O. A. Vydrov and T. Van Voorhis, *The Journal of Chemical Physics* **133**, 244103 (2010).
- [77] H. Peng, Z.-H. Yang, J. P. Perdew, and J. Sun, *Phys. Rev. X* **6**, 041005 (2016).
- [78] R. W. G. Wyckoff, *Interscience Publishers, New York*, 2nd edn (1958).
- [79] J. Tesch, P. Leicht, F. Blumenschein, L. Gagnaniello, M. Fonin, L. E. Marsoner Steinkasserer, E. Paulus, Beate Voloshina, and Y. Dedkov, *Scientific Reports* **6**, 23439 (2016).
- [80] G. Zhao, X. Li, M. Huang, Z. Zhen, Y. Zhong, Q. Chen, X. Zhao, Y. He, R. Hu, T. Yang, R. Zhang, C. Li, J. Kong, J.-B. Xu, R. S. Ruoff, and H. Zhu, *Chem. Soc. Rev.* **46**, 4417 (2017).
- [81] S. M. Song, J. K. Park, O. J. Sul, and B. J. Cho, *Nano Letters* **12**, 3887 (2012).
- [82] H. Yuan, S. Chang, I. Bargatin, N. C. Wang, D. C. Riley, H. Wang, J. W. Schwede, J. Provine, E. Pop, Z.-X. Shen, P. A. Pianetta, N. A. Melosh, and R. T. Howe, *Nano Letters* **15**, 6475 (2015).
- [83] A. Patra, J. E. Bates, J. Sun, and J. P. Perdew, *Proceedings of the National Academy of Sciences* **114**, E9188 (2017).